35th Annual International Conference of the IEEE EMBS
Osaka, Japan, 3 - 7 July, 2013

A Quantitative Analysis of F-Actin Features and Distribution in Fluorescence Microscopy Images to Distinguish Cells with Different Modes of Motility *

Jie Cheng, Xiaoping Zhu, Hao Cheng, Hong Zhao, Stephen T.C. Wong

Abstract— **Actin is one of the most abundant proteins in eukaryote cells, playing a key role in cell dynamic morphological alterations and tumor metastatic spread. To investigate the relationship between the distribution patterns of actin and the aggressiveness of cancer cells, we developed an image analysis framework for quantifying cell F-actin distributions examined with fluorescence microscopy. The images are first segmented with multichannel information of both F-actin and nuclear staining. Using the watershed method and Voronoi tessellation, the cells can be well segmented based on both F-actin and nuclear information. Altogether, sixteen F-actin distribution features are calculated for each individual cell. A linear Support Vector Machine (SVM) is then applied in the feature space to separate cells with different modes of motility. Our results show that cells with different modes of motility can be distinguished by F-actin distributions. To our knowledge, this is the first study managing to distinguish cancer cells with different aggressiveness based on quantitative analysis of F-actin distribution patterns.**

I. INTRODUCTION

Tumor progression is a complex process invoking multimodal parameters that enable tumor cells to evade host defense mechanisms and to migrate and establish new colonies or metastases [1]. Tumor metastasis is the main cause of death in cancer patients. It is crucial to understand the signaling mechanisms underlying the metastatic cascade of cancer and identify new cancer therapy treatments targeting invasion and metastasis.

Actin is one of the most abundant proteins in eukaryotes and participates in many important cellular processes. The microfilament system of actin plays a key role in cell dynamic morphological alterations. The reorganization and reassembly of the actin cytoskeleton are involved in almost all steps of metastatic spread. Dynamic actin cytoskeleton remodeling and stabilization of *de novo* substrate contacts drive pseudopodial protrusion and the formation of related invadopodia, which has long been associated with tumor cell migration and invasion [2-4]. Quantification of actin pattern changes is important for understanding the differences between cell types and for elucidation of cell functional changes. The effects and dynamics of drug interactions have been actively studied recently. In [5] C. Cui et al. studied the change of F-actin organization patterns in confocal microscopy images in response to different candidate pharmaceutical treatments. Q. Yi and M.G. Coppolino proposed an automatic method for quantitative comparison of cellular ruffle formation under different experimental conditions [6]. Here, we are more interested in distinguishing cells with different modes of motility (and thus aggressiveness) by quantitative analysis of their F-actin distributions. Our hypothesis is that the F-actin distribution patterns can effectively differentiate cancer cells based on their invasive aggressiveness.

In this paper, we have developed an image analysis framework for quantifying F-actin organization patterns in fluorescence microscopy images in response to two cancer cell types with different aggressiveness. The resultant numerical features are effective to quantitatively profile the changes in the spatial distribution of F-actin and facilitate the comparison of different cell types. The validation for the classification is done through visual inspection. To our knowledge, this is the first study managing to distinguish cancer cells with different aggressiveness based on quantitative analysis of F-actin distribution patterns. Section 2 describes the experimental conditions for image acquisition; Section 3 gives a brief introduction of the algorithms applied; Section 4 shows the experimental results; discussion and conclusion are presented in Sections 5 and 6, respectively.

II. IMAGE ACQUISITION

Images of two human mammary epithelial cell lines, viz. HMLE-vector and HMLE-snail were acquired. HMLE-Snail cells acquired fibroblast-like, mesenchymal appearances and became aggressive after over-expressing snail compared with HMLE-vector [7]. These two cell lines were fixed by 4% paraformaldehyde at room temperature for 15 min, then permeabilized by 0.2% Triton-X. After blocking 30 min with BSA, actin was stained in phalloidin for 30 min. After washing 3 times in phalloidin staining, cells were incubated with DAPI for 5 min. Samples were observed under

*Resrach supported by NIH U54CA149169 and NIH R01CA121225.

J. Cheng is with the Systems Medicine and Bioengineering Department, The Methodist Hospital Research Institute, Weill Cornell Medical College, Houston, TX 77030, USA

X. Zhu is with the Systems Medicine and Bioengineering Department, The Methodist Hospital Research Institute, Weill Cornell Medical College, Houston, TX 77030, USA

H. Cheng is with the Orthopedic Department, Tongji Hospital, Tongji Med. School, Huazhong University of Science& Technology, Wuhan, P. R. China 430030

H. Zhao is with the Systems Medicine and Bioengineering Department, The Methodist Hospital Research Institute, Weill Cornell Medical College, Houston, TX 77030, USA

S.T.C. Wong is with the Systems Medicine and Bioengineering Department, The Methodist Hospital Research Institute, Weill Cornell Medical College, Houston, TX 77030, USA (phone: 713-441-5884; fax: 713-441-8696; e-mail: stwong@tmhs.org).

fluorescence microscopy and we randomly picked three regions for image acquisition under each condition.

III. METHODOLOGY

The acquired 8-bit $M \times N$ size grey images can be described by matrix $I(x, y)$, viz. $\{I(x, y) | 1 \leq x \leq M, 1 \leq y \leq N, 0 \leq I(x, y) \leq 255\}$. Images are acquired in two channels: nuclear and F-actin fluorescence. To distinguish actin distributions of cells with different modes of mobility, the images are first segmented based on the multichannel information, following which, quantitative features of actin distributions are extracted. The Support Vector Machine (SVM) is trained and applied to classify the two cell types in the extracted feature space.

A. Segmentation

Both F-actin and nuclear images are initially segmented using the Otsu method, which exhaustively searches for the threshold minimizing the intra-class variance $\sigma_w^2(t)$:

$$\sigma_w^2(t) = w_1(t)\sigma_1^2(t) + w_2(t)\sigma_2^2(t), \quad (1)$$

where w_i and σ_i^2 are the probabilities and variance of the two classes, respectively; t is the threshold. The initial segmented foreground objects of actin (cell membrane) and nuclear images, namely, $I_c'$and $I_n'$are combined into I': $\{I' | I'(\text{foreground}) = I_c'(\text{foreground}) \cup I_n'(\text{foreground})\}$.

After initial segmentation, the cell blobs are detected. However, further processing is still needed to find the true boundaries of partially segmented cells and to separate cells adjacent to each other. Voronoi tessellation and the watershed method are applied here. Voronoi tessellation is a way of dividing space into a number of regions based on a set of seeds. For each seed there is a corresponding region consisting of all points closer to it than to any other seeds. If I' is the image to be processed, S_k is the k-th seed, i.e. the partially segmented cell; i is a pixel in the image, then the final segmented cell, viz. the k-thVoronoi region R_k can be defined as:

$$R_k = \{i \in I' | d(i, S_k) \leq d(i, S_j) \text{ for all } j \neq k\} \quad (2)$$

where d is the Euclidean distance.

Fig. 1 shows the F-actin and nuclear images for both HMLE-vector and HMLE-snail cells. For HMLE-vector cells shown in Fig. 1(a), the cells can be well separated because of the highlighted cell boundary regions. Only Voronoi tessellation is applied for further segmentation with the partially segmented cells set as the seeds. For HMLE-snail cells, cell boundaries can hardly be detected in F-actin images as shown in Fig. 1(b). The nuclei, as shown in Fig. 1(d), are set as the seeds. The watershed method is applied first to separate the attached nucleus. The final segmentation results are illustrated in Fig. 1(e) and Fig. 1(f).

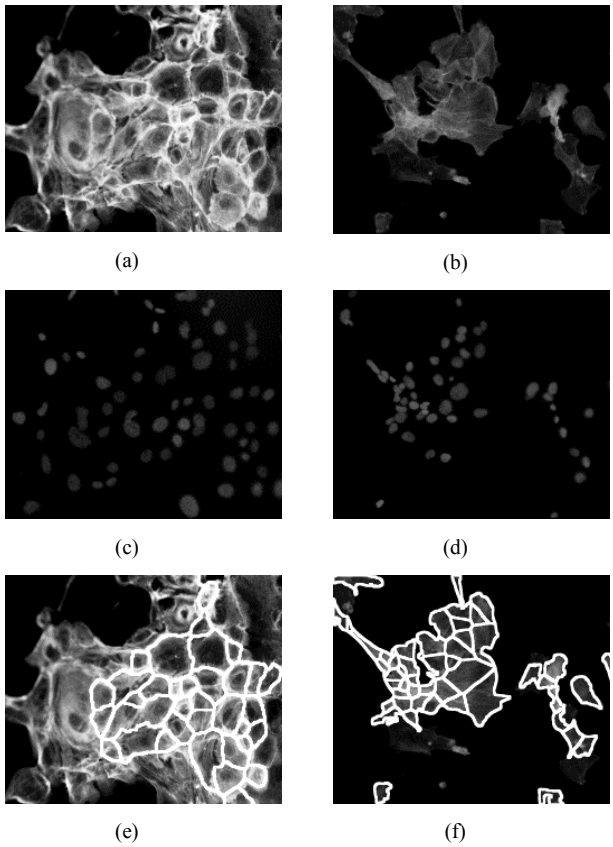

Figure 1. Segmentation results based on F-actin and nuclei images (a) F-actin image of HMLE-vector cell; (b) F-actin image of HMLE-snail cell; (c) nuclei image of HMLE-vector cell; (d) nuclear image of HMLE-snail cell; (e) segmentation result of (a); (f) segmentation results of (b).

B. Classification

To distinguish cells with different modes of motility based on quantitative actin distribution information, relevant features need to be extracted and tested by an optimal classifier. Here, altogether 15 measurements are selected: namely, the mean, mode, median, and standard deviation of F-actin in both cell boundary and nuclei regions; the ratios of the aforementioned four values between the above two kinds of regions; and the contrast, correlation, and entropy of F-actin in each individual cell. Suppose there are N pixels in a region R, the intensity value for the i-th pixel in the F-actin image is p_i, then Mean(R) = $\frac{1}{N}\sum_{i=1}^{N} p_i$, Mode(R) = $\{ p_i \mid p_i$ is the most frequent value in $R\}$, Median(R) = $\{ p_i \mid p_i$ is the middle value in $R\}$, SD(R) = $\sqrt{\frac{1}{N}\sum_{i=1}^{N}(p_i - mean(R))^2}$. The contrast, correlation, and entropy are defined by Eq. (3)-(5) respectively:

$$\text{Con(R)} = \sum_{x,y}(x - y)^2 v(x, y) \quad (3)$$

$$\text{Cor(R)} = \sum_{x,y} \frac{(x-\mu_x)(y-\mu_y)v(x,y)}{\sigma_x \sigma_y} \quad (4)$$

$$\text{Ent(R)} = \sum_{x,y} v(x,y)^2 \quad (5)$$

where $v(x,y)$is the (i,j)-th entry in the normalized co-occurrence matrix.

After the features are obtained, various classifiers can be used to distinguish different cell types in the feature space. The linear SVM, which is known as the best classifier in the sense of minimizing the probabilistic upper bound of the error on the test set, is applied here. Given training samples, a SVM can be trained to separate categories divided by a gap that is as wide as possible. New samples are classified in the same feature spaces based on the prediction of the trained SVM.

IV. EVALUATION OF RESULTS

Three HMLE-vector cell images and three HMLE-snail cell images were analyzed. Only cells at the edge of the clusters were analyzed, with a total number of 34 HMLE-vector cells and 41 HMLE-snail cells. For better illustration, the 15-D feature space was reduced to the 2-D space using principle component analysis (PCA). To train the SVM classifier, 50% of the 75 cells were randomly selected as the training data, with the remaining 50% cells as the test data. Figure 2 illustrates the result of one of the experiments. We can see that HMLE-vector and HMLE-snail cells can be successfully distinguished by a SVM classifier in a reduced 2-D feature space. With cross-validation, the experiment was repeated 10 times. Each time, 50% of the cells were randomly selected as the training data and the remaining 50% of cells as the test data. The overall average accuracy rate was 94%, with 83% and 100% for the worst and best cases, respectively.

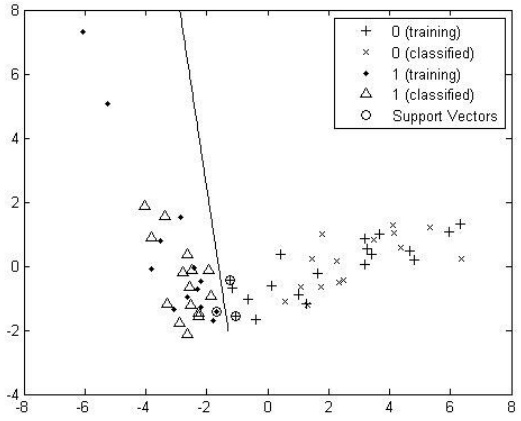

Figure 2. Classification of HMLE-snail and HMLE-vector cells in 2-D space after PCA. Here 0 and 1 represent the HMLE-vector and HMLE-snail cells, respectively.

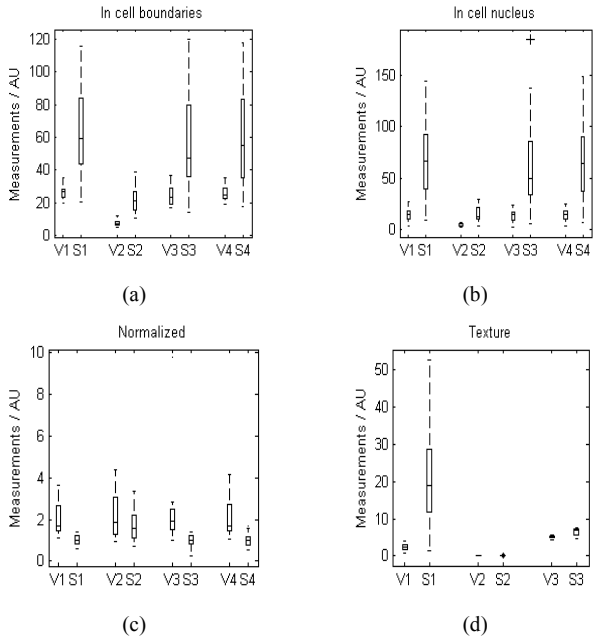

Figure 3. Comparison of the F-actin distributions between HMLE-vector and HMLE-snail cells: (a) measurements in cell boundaries, where V1-V4 are the mean, standard deviation, mode, and median intensity values of HMLE-vector cells; S1-S4 are the mean, standard deviation, mode and median intensity values of HMLE-snail cells, respectively; (b) measurements in cell nucleus regions; (c) normalized measurements, i.e. measurements in boundaries divided by measurements in nucleus; (d) texture of two types of cells, where V1-V3 and S1-S3 are the contrast, correlation, and entropy of HMLE-vector and HMLE-snail cells, respectively.

Figure 3 compares the F-actin distributions between HMLE-vector and HMLE-snail cells. As we can see from the results, the mean, standard deviation, mode, and median intensity values of HMLE-vector cells are much lower than those of HMLE-snail cells, in both boundary and nuclear regions. In contrast, the normalized values (measurements in boundaries divided by measurements in nucleus) of HMLE-vector cells are higher than those of HMLE-snail cells. As for the texture features, the contrast and entropy show different F-actin distribution patterns in two types of cells, while the correlation shows little difference.

V. DISCUSSION

Actin is a major component of the cell membrane and cytoskeleton, which plays a significant role in cell deformation and migration. It is important to understand how actin distribution patterns describe different cell behaviors. For example, to distinguish cells with different migration ability, such as HMLE-snail and HMLE-vector cells, normally genotypic data such as western blot are needed for the purpose of validation. However, if we can identify specific F-actin distribution patterns for different cell types, we can distinguish these cells directly from microscopic examination.

The F-actin distribution patterns can be described in various ways. As shown in Figure 3, some of the measurements (e.g. median and contrast) are more effective than others (e.g. normalized standard deviation and correlation) in cell differentiation. It would be interesting to study the mechanisms behind these actin distribution patterns shown in different cells. We believe that actin quantification from microscopic cell images can indeed provide some exciting insights on the factors affecting cell deformation, migration, and other cellular behaviors and functions, and thus help bridge the gap between the morphologic changes at the cellular level and the hidden mechanisms at the molecular level.

VI. Conclusion

The microfilament system of actin plays a key role in cell dynamic morphological alterations and is involved in almost all steps of metastatic spread. To find the relation between actin distribution patterns and aggressiveness of cancer cells, we developed an image analysis framework for quantifying F-actin in fluorescence microscopy images. The images are first segmented with multichannel fluorescence information of both F-actin and nuclei. The watershed method and Voronoi tessellation are then used for cell segmentation. Altogether, 15 features of the F-actin distributions are calculated based on the segmentation results. A linear SVM is applied in the feature space to separate two types of cancer cells in this study. The results show that the F-actin distribution patterns are closely related to modes of motility of different cells. Classifiers based on the F-actin distribution features can effectively distinguish cells with different modes of motility. Future work will include more detailed study of the relationship between the quantitative features of F-actin distribution and the modes of cell motility, e.g. identifying and quantifying features of actin at different locations such as cortical, puncturate, and stress fiber and validating the robustness and effectiveness of the extracted features.

References

[1] J. Shankar, *et al.*, "Pseudopodial actin dynamics control epithelial-mesenchymal transition in metastatic cancer cells," *Cancer Research,* vol. 70, pp. 3780-90, 2010.

[2] R. Guirguis, *et al.*, "Cytokine-induced pseudopodial protrusion is coupled to tumour cell migration," *Nature,* vol. 329, pp. 261-3, 1987.

[3] W. T. Chen, "Proteolytic activity of specialized surface protrusions formed at rosette contact sites of transformed cells," *The Journal of experimental zoology,* vol. 251, pp. 167-85, 1989.

[4] T. D. Pollard and G. G. Borisy, "Cellular motility driven by assembly and disassembly of actin filaments," *Cell,* vol. 112, pp. 453-65, 2003.

[5] C. Cui, *et al.*, "Quantifying the astrocytoma cell response to candidate pharmaceutical from F-ACTIN image analysis," *Conference proceedings : Annual International Conference of the IEEE Engineering in Medicine and Biology Society IEEE Engineering in Medicine and Biology Society Conference,* vol. 2009, pp. 5768-71, 2009.

[6] Q. Yi and M. G. Coppolino, "Automated classification and quantification of F-actin-containing ruffles in confocal micrographs," *BioTechniques,* vol. 40, pp. 745-6, 748, 750 passim, 2006.

[7] S. A. Mani, *et al.*, "The epithelial-mesenchymal transition generates cells with properties of stem cells," *Cell,* vol. 133, pp. 704-15, 2008.